Frontiers in Bioscience Landmark

Front. Biosci. (Landmark Ed) **2026**; 31(2): 45159
https://doi.org/10.31083/FBL45159

Original Research

METTL16 Modulates GPX4 Expression to Regulate Chondrocyte Ferroptosis

Li He[1,†], Xing Tong[2,†], Ming Yang[2], Xiaoming Wang[2], Xiaowei Wang[2], Bing Wang[2,*]

[1]Department of Child Healthcare, The Affiliated Children's Hospital of Xi'an Jiaotong University (Xi'an Children's Hospital), 710003 Xi'an, Shaanxi, China
[2]Pediatric Orthopaedic Hospital, Honghui Hospital, Xi'an Jiaotong University, 710054 Xi'an, Shaanxi, China
*Correspondence: Wangbingheli@163.com (Bing Wang)
[†]These authors contributed equally.

Academic Editor: Emerito Carlos Rodriguez-Merchan
Submitted: 10 March 2025 Revised: 17 December 2025 Accepted: 23 December 2025 Published: 3 February 2026

Abstract

Background: Achondroplasia (ACH), the predominant inherited form of disproportionate short stature, results from specific genetic alterations in fibroblast growth factor receptor 3 (FGFR3). N6-methyladenosine (m^6A) modification is reported to modulate mRNA stability and translation. The present investigation systematically explored the epigenetic regulatory function of *METTL16*, an m^6A RNA methyltransferase, within the pathophysiological framework of ACH. **Methods**: We generated an ACH mouse model via *Fgfr3380R* (*Fgfr3*^{ach}) gene mutation. Primary chondrocytes were isolated from newborn mice and stimulated with IL-1β to induce cell death. Proximal tibia tissues were collected and analyzed with HE staining, toluidine blue staining, safranin O staining, and immunohistochemical (IHC) analysis. Bone structure was analyzed by measuring bone mineral density (BMD), ratio of bone volume to total tissue volume (BV/TV), trabecular number (TbN), and trabecular thickness (TbTh). Cell viability and proliferation were assessed using the Cell Counting Kit-8 (CCK-8) and colony formation assays. The levels of iron (Fe^{2+}), malondialdehyde (MDA), and glutathione (GSH) were measured to assess ferroptosis. Protein and RNA levels were measured by western blotting and quantitative real-time PCR (qPCR) assay, respectively, while the m^6A modification level was assessed by m^6A mRNA immunoprecipitation (IP). **Results**: METTL16 improved bone chondrogenesis in the ACH mouse model, with METTL16 overexpression promoting the proliferation of primary chondrocytes. METTL16 decreased ferroptosis both *in vitro* and *in vivo* and increased glutathione peroxidase 4 (GPX4) expression. METTL16 enhanced m^6A modification of GPX4 mRNA and suppressed its degradation. Depletion of GPX4 abolished the effects of METTL16 on ACH mice and chondrocytes. **Conclusion**: Overexpression of *METTL16* improved bone growth and alleviated ferroptosis of chondrocytes by increasing m^6A modification of GPX4 mRNA and thus GPX4 expression in chondrocytes. The METTL16/GPX4 axis may be a promising therapeutic approach for ACH treatment.

Keywords: achondroplasia; N6-methyladenosine; *METTL16*; chondrocyte; ferroptosis; *GPX4*

1. Introduction

Achondroplasia (ACH) is a condition resulting from a missense mutation in the fibroblast growth factor receptor 3 (*FGFR3*) gene. ACH is the leading cause of short stature in humans [1,2]. It is passed down through an autosomal dominant inheritance pattern, leading to the presentation of ACH-related symptoms in carriers of the FGFR3 mutation [3]. Despite advances in research, many preventative, diagnostic, and therapeutic challenges remain with ACH [4].

Ferroptosis is a recently identified form of oxidative cell death marked by the iron-dependent build-up of lipid peroxides to toxic levels [5]. It has become an effective target for avoiding multiple types of cancers and degenerative conditions, such as Alzheimer's disease, Parkinson's disease, and kidney degeneration [6–8]. Several proteins have been recognized as essential regulators of ferroptosis, including glutathione peroxidase 4 (GPX4), which regulates the production of glutathione (GSH), and the cysteine/glutamate antiporter SLC7A11, which promotes the import of cysteine for GSH biosynthesis and antioxidant defense [9,10]. Research has shown that maintaining a balance between anabolic and catabolic processes in cartilage, as well as the survival of chondrocytes, is essential for the health of articular cartilage and for preventing the progression of osteoarthritis. This underscores the importance of chondrocyte regulation for articular cartilage health.

Epigenetic regulatory processes, including DNA methylation and N6-methyladenosine (m^6A), are exciting new areas of investigation in the field of tumor biology [11]. m^6A modification can selectively modulate polyadenylation and pre-mRNA splicing, thereby regulating mRNA stability and translation [12,13]. m^6A modification is the most prevalent modification after transcription, and is primarily mediated by m^6A "writers", "erasers", and "readers" (WER) [14]. The m^6A methylation of RNA is mediated by a multiprotein complex and initiated by methyltransferases such as methyltransferase-like 3 (METTL3), METTL14, METTL16, and WTAP (WT1-associated proteins). Moreover, it is modulated by "erasers" includ-

ing AlkB congeners, demethylase FTO (α-ketoglutarate-dependent dioxygenase FTO), and RNA demethylases, as well as "readers" such as YTH N6-methyladenosine RNA-binding protein 1 (YTHDF1) and YTHDF3 that recognize m^6A-modified RNA and promote mRNA translation [15,16].

In this study, we explored the role of METTL16 in ACH and investigated m^6A-regulated ferroptosis during ACH development. Our findings reveal a novel and promising mechanism for the prevention and treatment of ACH.

2. Materials and Methods

2.1 Mouse Model

Transgenic mice with a C57BL/6 background and carrying the heterozygous *Fgfr3*^{ach} transgene were obtained from Shanghai Model Organisms (China). They were housed in SPF conditions with free access to water and food. The mean bodyweight of mice at 8 weeks of age was approximately 20 g. Mouse genotypes were ascertained by qPCR. Wild-type C57BL/6 mice were used as controls. For all procedures involving tissue harvesting, mice were first anesthetized using isoflurane (2% for induction, 1.5% for maintenance) delivered via a precision vaporizer (2V22105103, RWD Life Science Co., Ltd., Shenzhen, Guangdong, China), ensuring a consistent and humane depth of anesthesia. Following anesthesia, mice were euthanized by cervical dislocation to minimize suffering and ensure ethical compliance. For treatment, lentivirus with METTL16 overexpression vectors (pCDH-CMV vectors; GenePharma, Shanghai, China) was intraperitoneally injected into newborn mice for 20 days. The tibiae from mice were collected and processed into paraffin-embedded samples or stored in liquid nitrogen for subsequent experiments. All animal procedures were approved by the Institutional Animal Care and Use Committee (IACUC) of Animal Care and Use Committee of Pediatric Orthopaedic Hospital, Honghui Hospital, Xi'an Jiaotong University (No. KT2023-01-05-01) and conducted in accordance with the relevant guidelines and regulations.

2.2 Cell Culture and Treatment

Chondrocytes were prepared from the tibia of newborn mice [17] and cultured in DMEM medium with 10% fetal bovine serum (FBS) in a 37 °C incubator. Cell transfection was conducted using Lipofectamine 2000 (11668027, Invitrogen™, Carlsbad, CA, USA) for 48 h. Chondrocytes were stimulated with IL-1β (10 µg/mL) for 6 h to induce cell death and apoptosis.

All primary chondrocytes were freshly isolated and used at early passage. STR authentication is not applicable to primary cells.

Primary cells were observed daily under a phase-contrast microscope. The cells exhibited typical morphology consistent with human nucleus pulposus/endplate chondrocyte characteristics, including a polygonal or round shape, relatively large nuclei, and a pericellular lacuna-like structure. No fibroblast-like overgrowth or abnormal morphological changes were observed within passages P2–P4, which were used for subsequent experiments.

2.3 Measurement of Bone Parameters

The micro-architecture parameters of the tibia from mice were analyzed by assessing the bone mineral density (BMD), bone volume to total tissue volume (BV/TV), trabecular number (TbN), and trabecular thickness (TbTh).

2.4 Histological Examination

For histological examination, tibial tissues were preserved in 10% formalin, demineralized using 0.5 M EDTA, embedded in paraffin, and then cut into 5 µm sections. The histomorphology was observed by staining with hematoxylin and eosin (H&E; C0105S, Beyotime, Shanghai, China). The expression of METTL16 was assessed by immunohistochemical (IHC) staining using anti-METTL16 antibody (17676, Cell Signaling Technology, Danvers, MA, USA, 1:1000) and visualized by DAB (Beyotime, China) as the substrate.

2.5 Toluidine Blue Staining

The samples were stained with toluidine blue (89640, Sigma, St. Louis, MO, USA). This stains cartilage and osteoblasts a dark blue color against a light blue background.

2.6 Safranin O Staining

Bone samples were stained with safranin O solution, Weigert hematoxylin solution, and solid green staining solution (Sigma, USA). This results in chondrocyte cytoplasm presenting as red, and chondrocyte nuclei presenting as gray black.

2.7 Cell Counting Kit 8 (CCK-8)

Cells induced by IL-1β and transfected with METTL16 overexpression vectors were seeded into 96-well plates and cultured for 24 h. At the final time point, CCK-8 reagent (C0005, TargetMol, Shanghai, China) was added to each well and reacted for 2 h. The absorbance values at 450 nm were then measured, and the relative cell viability was calculated.

2.8 Colony Formation

Chondrocytes were digested into a single cell suspension and seeded into 6-well plates at a density of 10,000 cells per well. After incubation for 10 days, the colonies were stained with crystal violet (Sigma, USA) for 20 min, and the images were recorded with a camera.

2.9 Detection of Ferroptosis

The concentration of malondialdehyde (MDA), which is the final product of lipid peroxidation, was determined using a lipid peroxidation assay kit (Doojindo, Kumamoto,

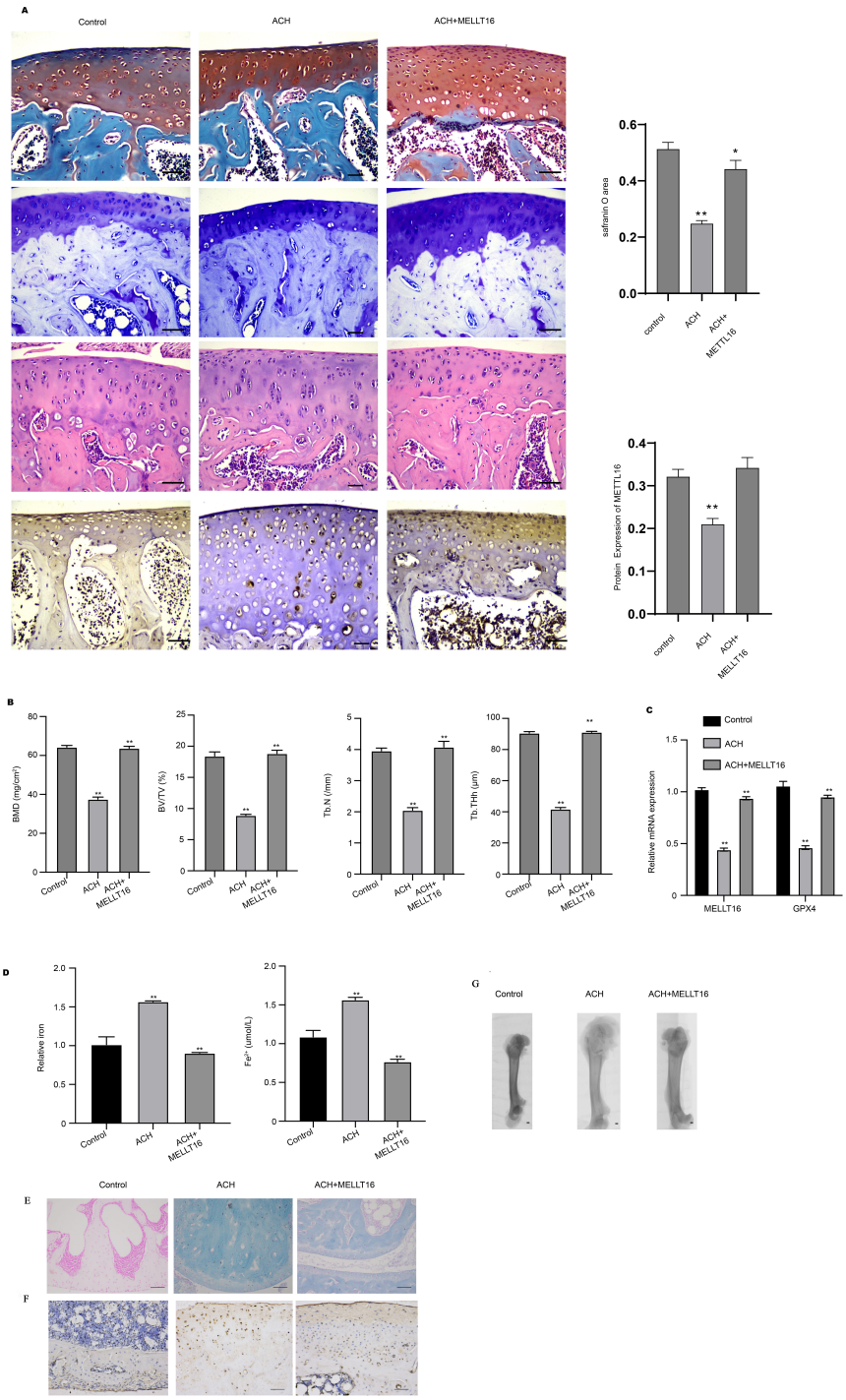

Fig. 1. METTL16 promotes bone chondrogenesis and suppresses ferroptosis in the ACH mouse model. *Fgfr3*^{ach} transgenic mice were treated with METTL16 lentivirus, and the proximal tibia tissues were collected for analysis. (A) The morphology of cartilage, chondrocyte, and tissues was examined by toluidine blue, safranin O, and H&E staining, while the expression of METTL16 was examined by IHC. Scale bar = 100 μm. (B) Results for bone mineral density (BMD), bone structure via the bone volume to total tissue volume ratio (BV/TV), trabecular number (TbN), and trabecular thickness (TbTh). (C) RNA levels of METTL16 and GPX4, as measured by qPCR assay. (D) The levels of total iron and Fe^{2+} were measured to assess ferroptosis. (E) Representative Perls' Prussian blue staining of tibial sections showing iron deposition (blue). Quantitative analysis of Perls-positive area. Scale bar = 100 μm. (F) Representative IHC staining for 4-HNE showing the levels of lipid peroxidation in tibiae. Quantitative analysis of 4-HNE–positive signal intensity. Scale bar = 100 μm. (G) CT reconstruction for observing the microstructure of bone cartilage in ACH mice. Scale bar = 100 μm. $^{**}p < 0.01$, $^{*}p < 0.05$. ACH, Achondroplasia; H&E, hematoxylin and eosin; IHC, immunohistochemical; GPX4, glutathione peroxidase 4; qPCR, quantitative real-time PCR; 4-HNE, 4-Hydroxynonenal; CT, computed tomography.

Japan). Additionally, total iron and Fe^{2+} levels were evaluated with an iron assay kit (ab83366, Abcam, Woburn, MA, USA), as per the instructions provided by the manufacturer.

2.10 Western Blot Assay

Cell lysates were obtained using RIPA buffer (89900, Invitrogen™, Carlsbad, CA, USA). Following loading and separation on an SDS-PAGE gel, the proteins were transferred to PVDF membranes and blocked with 5% skim milk. The membranes were then incubated overnight at 4 °C with primary antibodies against METTL16 and GPX4 (1:1000, ab252420; ab125066, Abcam, USA). They were subsequently treated with HRP-conjugated anti-rabbit secondary antibodies (1:1000, ab6721, Abcam, USA), and protein bands were visualized using an ECL chemiluminescence substrate (WBKLS0500-2, Millipore, Burlington, MA, USA).

2.11 Quantitative Real-Time PCR (qPCR) Assay

Tissues and chondrocytes were treated with Trizol reagent to isolate total RNA. This was converted into cDNA using the PrimeScript RT reagent kit (RR037A, Takara, Kyoto, Japan). Real-time qPCR was performed with the SYBR Green qPCR Master Mix (Thermo, Waltham, MA, USA). Gene expression levels were measured relative to the β-actin gene as an endogenous control.

2.12 m^6A mRNA Immunoprecipitation (IP) and Quantification

RNAs were isolated from cells and incubated with protein G beads (70024, CST, Danvers, MA, USA) that had previously been reacted with anti-m^6A monoclonal antibody at 4 °C for 12 h in rotation. After reaction at 4 °C for 6 h, the beads were eluted and washed, and RNA was extracted using Trizol. The level of METTL16 was measured by qPCR assay.

2.13 Statistical Analyses

Statistical analyses were conducted using GraphPad Prism 7.0 software (GraphPad Software, Inc,San Diego, CA, USA). The paired Student's *t*-test was utilized to compare two groups. For analyzing differences among multiple groups, either a one-way Analysis of Variance with Tukey's post hoc test or a Mann–Whitney U test was employed. The criterion for statistical significance was defined as $p < 0.05$.

3. Results

3.1 METTL16 Promotes Bone Chondrogenesis and Suppresses Ferroptosis in the ACH Mouse Model

We first examined the *in vivo* effects of METTL16 on ACH using transgenic mice. The expression of METTL16 was suppressed in the proximal tibia of ACH mice compared with the control, but was recovered by treatment for METTL16 overexpression (Fig. 1A). Further analysis of the proximal tibia revealed an increased number of chondrocytes and cartilage, as well as an organized tissue structure after METTL16 overexpression compared with ACH mice (Fig. 1A). Treatment with METTL16 overexpression vectors also increased the BMD, BV/TV, TbN and TbTh compared to ACH (Fig. 1B). Notably, the expression of METTL16 and GPX4 were suppressed in the tibia tissues of ACH mice, while METTL16 overexpression recovered the levels of both (Fig. 1C). This observation suggests a potential correlation between the two genes and participation in ferroptosis during ACH. We next investigated the level of ferroptosis in the tibia of mice. The elevated levels of total iron and Fe^{2+} in the ACH group compared with the control group indicated an increase in cell ferroptosis. This was suppressed upon METTL16 overexpression (Fig. 1D). Perls' Prussian blue staining demonstrated minimal iron deposition in control tibiae, whereas ACH mice exhibited prominent deposits concentrated in the growth plate and trabecular regions. Quantitative image analysis confirmed a significantly larger Perls'-positive area in ACH mice compared with controls, which was significantly reduced by METTL16 overexpression (Fig. 1E). In line with this, IHC for 4-Hydroxynonenal (4-HNE) showed markedly elevated lipid peroxidation in ACH tibiae, with intense cytoplasmic and extracellular 4-HNE staining. Overexpression of METTL16 substantially decreased this 4-HNE positivity (Fig. 1F). These histological findings, together with increased tissue iron and Fe^{2+} levels and decreased GPX4 expression in ACH, indicate enhanced ferroptosis in ACH that can be alleviated by restoring METTL16 expression. To further delineate the therapeutic effects of METTL16 on bone microstructure and cartilage morphology, we performed micro-computed tomography (CT) reconstruction of the proximal tibiae (Fig. 1G). CT analysis revealed that ACH mice exhibited severe trabecular bone deterioration, characterized by fragmented, disconnected trabeculae with reduced spatial continuity. However, METTL16 overexpression substantially restored the integrity of the trabecular network.

3.2 METTL16 Overexpression Alleviates IL-1β–Induced Ferroptosis in Chondrocytes

To further examine whether ferroptosis is a major form of regulated cell death in chondrocytes and to confirm the protective role of METTL16, we employed specific inhibitors of ferroptosis (Ferrostatin-1) and apoptosis (Z-VAD-FMK) in a model of IL-1β-induced chondrocyte injury. The experimental groups comprised the control, IL-1β, IL-1β + METTL16 overexpression (OE), IL-1β + Ferrostatin-1, and IL-1β + Z-VAD-FMK. Cell viability, as determined by CCK-8 assay, was markedly reduced after IL-1β stimulation compared to the control group, indicating severe cellular injury. Both METTL16 OE and Ferrostatin-1 treatment significantly restored cell viability, whereas Z-VAD-FMK exerted only a minor protective effect (Fig. 2A). Lipid peroxidation, assessed using

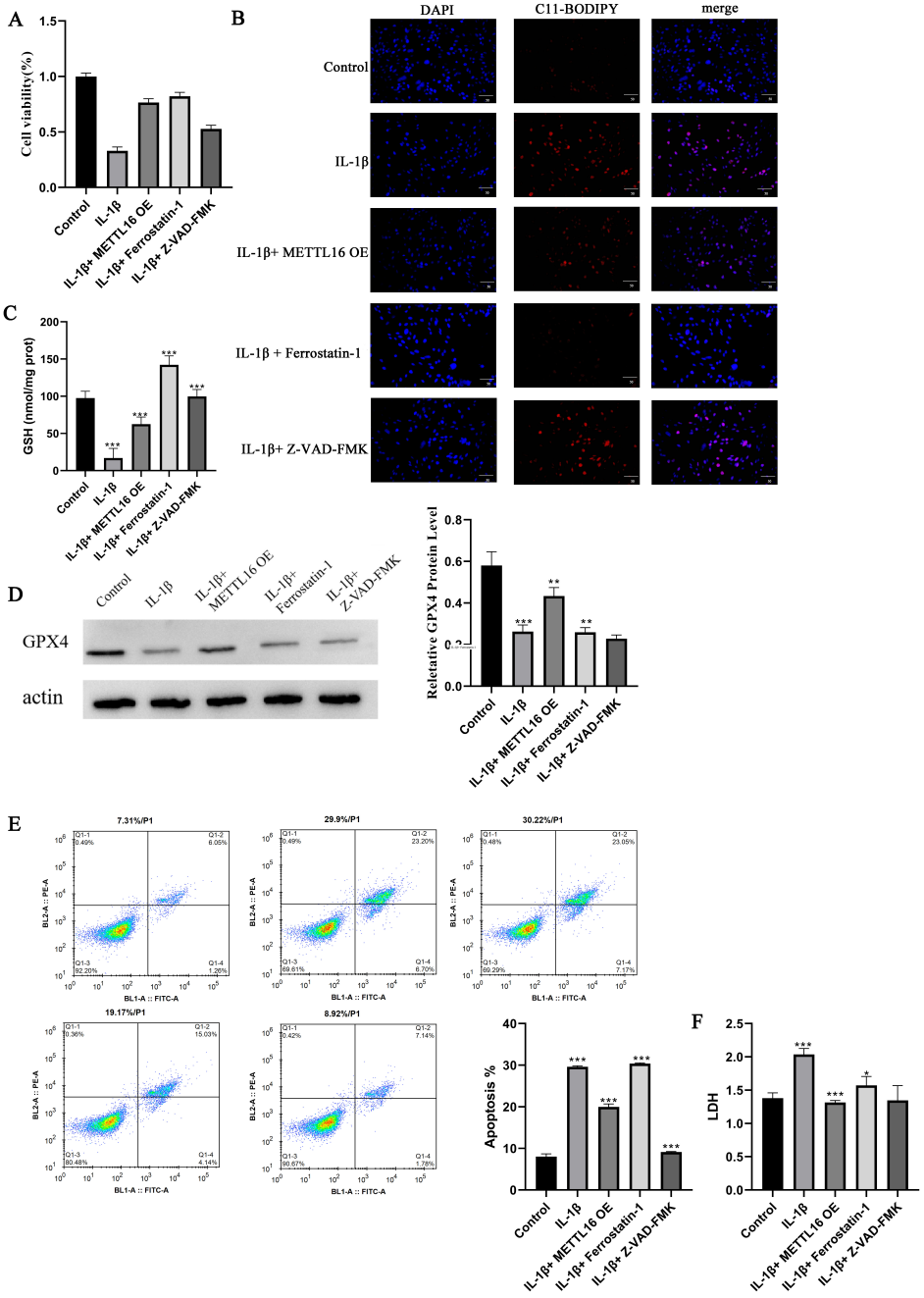

Fig. 2. METTL16 protects chondrocytes from IL-1β-induced injury primarily by inhibiting ferroptosis. (A) Cell viability assessed by CCK-8 assay in control, IL-1β, IL-1β + METTL16 OE, IL-1β + Ferrostatin-1, and IL-1β + Z-VAD-FMK groups. (B) Lipid peroxidation detected by C11-BODIPY fluorescence imaging and quantitative analysis. Scale bar = 50 µm. (C) Intracellular glutathione (GSH) levels in each group. (D) Western blot analysis and quantification of GPX4 protein expression. (E) Annexin V/PI staining showing the percentage of apoptotic and necrotic cells. (F) Lactate dehydrogenase (LDH) release indicates cell membrane integrity. Data are presented as the mean ± SD (n = 3). ***$p < 0.001$, **$p < 0.01$, *$p < 0.05$. CCK-8, cell counting kit 8; IL-1β, interleukin-1 beta.

C11-BODIPY fluorescence, was significantly higher in IL-1β-treated chondrocytes, confirming enhanced oxidative stress. The elevated C11-BODIPY oxidation ratio was markedly decreased by METTL16 OE and Ferrostatin-1, but not by Z-VAD-FMK (Fig. 2B), suggesting a ferroptosis-dominant phenotype. In accordance with this, the GSH level was significantly reduced, and GPX4 protein expression was downregulated in the IL-1β group. Both METTL16 OE and Ferrostatin-1 markedly restored intracellular GSH and GPX4 levels, whereas Z-VAD-FMK showed negligible effects (Fig. 2C,D). In addition, Annexin V/PI staining demonstrated that IL-1β treatment in-

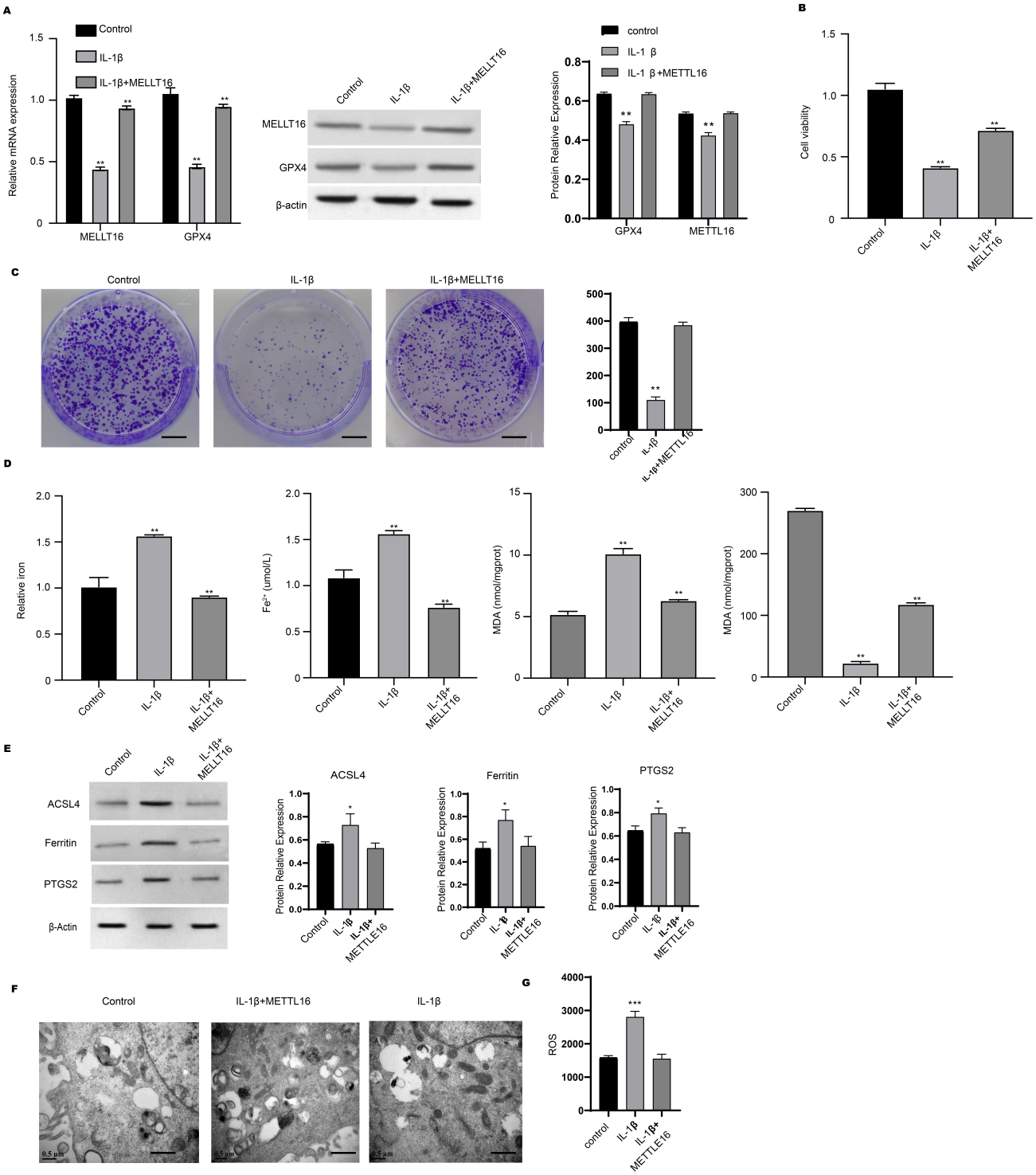

Fig. 3. METTL16 enhances chondrocyte proliferation and suppresses cell ferroptosis. Primary chondrocytes were stimulated with IL-1β and transfected with METTL16 overexpression vectors. (A) The RNA and protein levels of METTL16 and GPX4 were measured by qPCR and Western blot assays. (B) Cell viability was measured by the CCK-8 assay. (C) Cell proliferation was detected by colony formation. Scale bar = 100 µm. (D) The levels of iron, Fe^{2+}, MDA, and GSH were measured to assess ferroptosis. (E) Protein levels of ACSL4, Ferritin, and PTGS2, as measured by Western blot assay. (F) TEM analysis of mitochondrial ultrastructure in IL-1β-stimulated chondrocytes. Scale bar = 200 µm. (G) ROS levels as detected by the reagent kit. ***$p < 0.001$, **$p < 0.01$, *$p < 0.05$. MDA, malondialdehyde; ACSL4, Acyl-CoA synthetase long-chain family member 4; PTGS2, prostaglandin-endoperoxide synthase 2; TEM, transmission electron microscopy; ROS, reactive oxygen species.

duced a significant increase in Annexin V^+/PI^+ cells, indicating cell death. METTL16 OE and Ferrostatin-1 significantly reduced the proportion of Annexin V^+/PI^+ cells. LDH release, which is an indicator of membrane damage, was markedly elevated in IL-1β-treated cells. The increase in LDH was significantly attenuated by METTL16 OE and Ferrostatin-1, but remained largely unchanged with Z-VAD-FMK (Fig. 2E,F). Together, these findings demonstrate that IL-1β induces ferroptosis-like cell death in chondrocytes, characterized by lipid peroxidation, GSH depletion, and GPX4 downregulation. Both METTL16 overexpression and the ferroptosis inhibitor Ferrostatin-1 effectively alleviated these effects, confirming that METTL16 protects chondrocytes primarily by inhibiting ferroptosis rather than apoptosis. To further clarify the specificity of ferroptosis in IL-1β-induced chondrocyte death, we evaluated the contribution of autophagy using the pharmacological inhibitor 3-methyladenine (3-MA, 5 mM). IL-1β stimulation was found to induce autophagy, as evidenced by increased LC3B-II and decreased p62 levels. However, pretreatment with 3-MA effectively blocked LC3B-II accumulation but failed to restore cell viability (CCK-8 assay) or reduce ferroptosis markers (Fe^{2+}, MDA, GSH) (**Supplementary Fig. 1A–C**). METTL16 overexpression retained its protective effects in the presence of 3-MA. These data indicate that although autophagy is activated in IL-1β-stimulated chondrocytes, it does not represent the major form of regulated cell death, supporting ferroptosis as the dominant pathway.

3.3 METTL16 Enhances Chondrocyte Proliferation and Suppresses Cell Ferroptosis

Subsequently, we investigated the effects of METTL16 on chondrocytes. Cells from primary culture were treated with IL-1β to reduce viability and induce ferroptosis. As shown in Fig. 3A, treatment with IL-1β decreased the RNA and protein levels of METTL16 and GPX4, respectively, consistent with results from the *in vivo* experiments. Results from the CCK-8 and colony formation assays showed that overexpression of METTL16 could rescue the cell viability and proliferation of IL-1β-induced primary chondrocytes (Fig. 3B,C). Moreover, the status of several ferroptosis biomarkers, including elevated iron, Fe^{2+}, and MDA, and decreased GSH level, was significantly reversed by METTL16 overexpression (Fig. 3D). We next examined key protein markers to further investigate the mechanism by which METTL16 regulates ferroptosis. Western blot analysis revealed that IL-1β stimulation significantly upregulated the pro-ferroptotic proteins ACSL4 and PTGS2, while downregulating the iron storage protein ferritin. Notably, METTL16 overexpression effectively reversed these aberrant protein expressions (Fig. 3E). Furthermore, overexpression of METTL16 significantly inhibited the reactive oxygen burst induced by IL-1β (Fig. 3F) and restored mitochondrial ultrastructure (Fig. 3G). Transmission electron microscopy revealed that IL-1β treatment caused marked mitochondrial swelling, loss or fragmentation of cristae, and increased electron density, all of which are characteristic features of ferroptosis. Quantitative analysis showed a significant increase in the proportion of swollen mitochondria and cristae-deficient mitochondria in the IL-1β group, which was markedly reduced upon METTL16 overexpression.

3.4 METTL16 Regulates the m^6A Modification and Degradation of GPX4 mRNA

To investigate how METTL16 influences GPX4 expression, we assessed the m^6A methylation levels of GPX4 mRNA. The reduction of METTL16 levels using siRNAs was found to markedly decrease m^6A modification of GPX4 mRNA (Fig. 4A). Moreover, depletion of METTL16 decreased the protein level of GPX4 (Fig. 4B). We also utilized CHX to block protein synthesis. The protein level of GPX4 was notably decreased 6 h after CHX treatment, and depletion of METTL16 induced faster degradation of GPX4 (Fig. 4C). These results indicate that knockdown of METTL16 can reduce the stability of GPX4 mRNA.

3.5 METTL16 Overexpression and Inhibition of Ferroptosis Reduce Cartilage Degeneration in ACH Mice

To further validate the involvement of ferroptosis in ACH pathology and clarify the therapeutic potential of METTL16, ACH mice were treated with METTL16 overexpression (OE) vectors, the ferroptosis inhibitor Ferrostatin-1 (Fer-1, 1 mg/kg i.p.), or Caspase inhibitor/Necrostatin-1 (Casp/Nec-1). Normal mice served as controls. Proximal tibiae and vertebrae were analyzed histologically and biochemically to assess ferroptosis and inflammation. H&E staining revealed that ACH mice exhibited a disorganized growth plate, reduced cartilage thickness, and decreased chondrocyte density compared with control animals. These pathological alterations were markedly attenuated by METTL16 OE and Fer-1 treatment, whereas Casp/Nec-1 intervention resulted in minimal improvement. Perls' Prussian blue staining revealed extensive iron accumulation in the trabecular and growth plate regions of ACH tibiae, which was significantly reduced in METTL16 OE- and Fer-1-treated mice (Fig. 5A). IHC for 4-HNE showed pronounced lipid peroxidation in ACH mice, reflected by intense cytoplasmic and extracellular staining, which was substantially alleviated by METTL16 OE and Fer-1 (Fig. 5B). Biochemical assays further supported these observations, with MDA and Fe^{2+}/total iron levels being significantly elevated, while GSH content was reduced in ACH mice. Both METTL16 OE and Fer-1 normalized these parameters, whereas Casp had little effect (Fig. 5C). Western blot analysis revealed marked downregulation of GPX4 and SLC7A11, and upregulation of the pro-ferroptotic proteins ACSL4 and transferrin receptor (TfR1) in ACH tissues. METTL16 OE and Fer-1 ef-

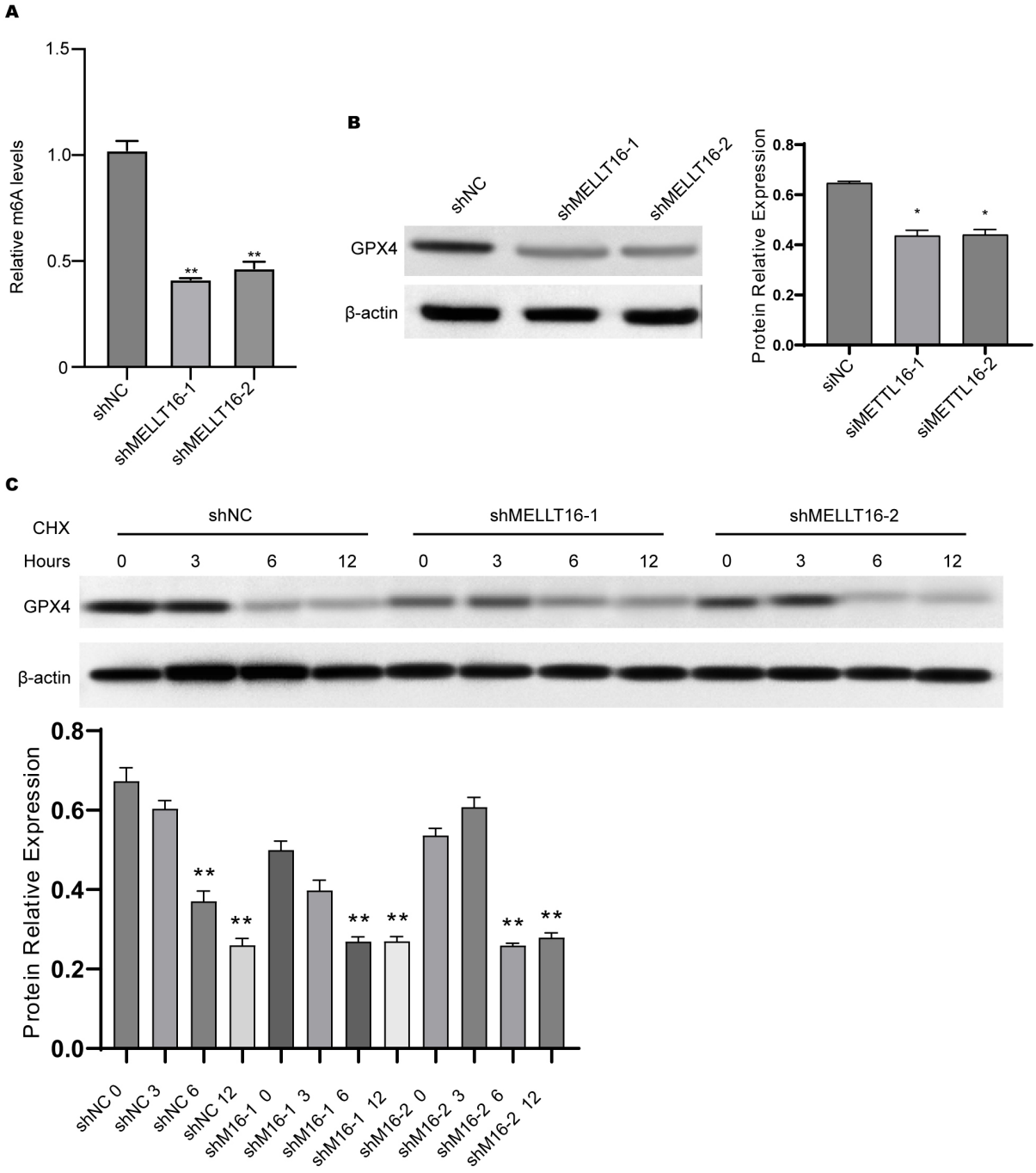

Fig. 4. METTL16 regulates m^{6}A modification and degradation of GPX4 mRNA. (A) The level of m^{6}A modification of GPX4 mRNA was measured by the m^{6}A mRNA IP assay. (B) The protein level of GPX4 in chondrocytes was measured by Western blotting. (C) Chondrocytes were first transfected with siMETTL16-1 or siMETTL16-2 and then treated with CHX, an inhibitor of protein synthesis. The protein level of GPX4 at 0, 3, 6, and 12 h after CHX treatment was assessed by Western blot assay. $^{**}p < 0.01$, $^{*}p < 0.05$.

fectively restored GPX4, SLC7A11 and ferritin (FTH1) expression, while reducing ACSL4 and TfR1 levels (Fig. 5D). Furthermore, serum and tissue cytokine analyses showed that TNF-α and IL-6 levels were markedly increased in ACH mice, while METTL16 OE and Fer-1 significantly reduced these inflammatory markers (Fig. 5E). Collectively, these data demonstrate that METTL16 overexpression and ferroptosis inhibition (Fer-1) effectively alleviate iron accumulation, lipid peroxidation, mitochondrial damage, and inflammation in ACH, whereas inhibition of apoptosis or necroptosis (Casp/Nec-1) exerts only limited effects, confirming that ferroptosis is the dominant form of regulated cell death in ACH.

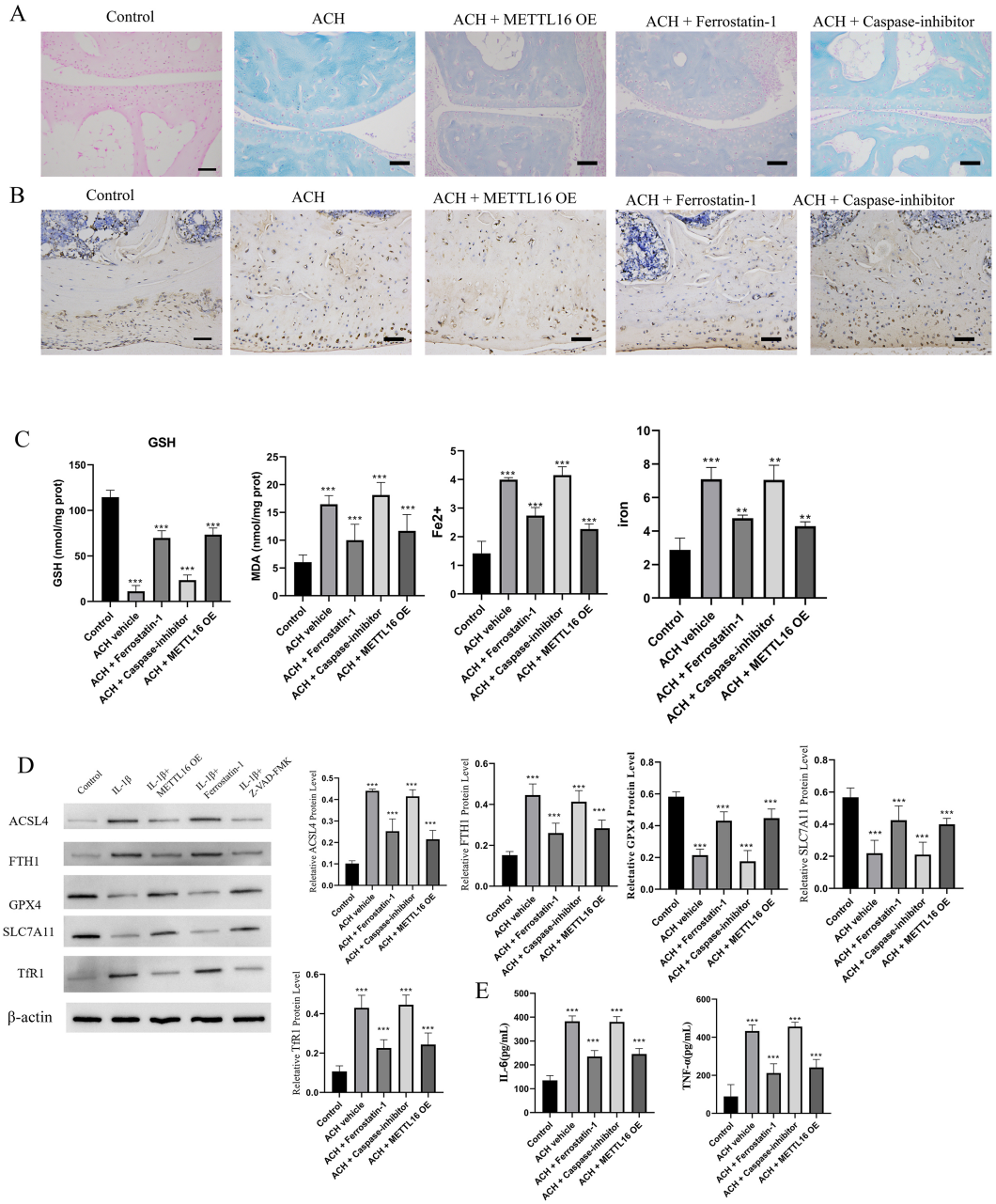

Fig. 5. METTL16 overexpression and ferroptosis inhibition alleviate ferroptosis and cartilage degeneration in ACH mice. (A) Perls' Prussian blue staining of proximal tibia sections showing iron accumulation in the trabecular and growth plate regions of ACH mice. Iron deposition was significantly reduced in groups with METTL16 overexpression (OE) and Ferrostatin-1 (Fer-1) treatment, whereas Caspase inhibitor (Casp) and Necrostatin-1 (Nec-1) treatment had minimal effects. Scale bar = 100 µm. (B) Immunohistochemistry for 4-HNE showed lipid peroxidation in ACH tibiae. Intense cytoplasmic and extracellular 4-HNE staining was observed in ACH mice, which was substantially reduced in METTL16 OE and Fer-1-treated groups. Scale bar = 100 µm. (C) Biochemical assays were used to measure MDA (malondialdehyde) and the Fe^{2+}/total iron ratio, as well as GSH (glutathione) content. Both METTL16 OE and Fer-1 restored MDA, Fe^{2+}/total iron levels, and GSH content to near normal levels, whereas Casp/Nec-1 treatment had little effect. (D) Western blot analysis of ferroptosis-related proteins in ACH tibiae. GPX4, SLC7A11, and ferritin (FTH1) were downregulated in ACH mice and restored by METTL16 OE and Fer-1, whereas ACSL4 and transferrin receptor (TfR1) were upregulated in ACH mice and reduced by METTL16 OE and Fer-1 treatment. (E) Serum and tissue inflammatory cytokine levels (TNF-α and IL-6) were measured by ELISA. METTL16 OE and Fer-1 significantly reduced the elevated levels of TNF-α and IL-6 in ACH mice, while Casp/Nec-1 had minimal effects. ***$p < 0.001$, **$p < 0.01$.

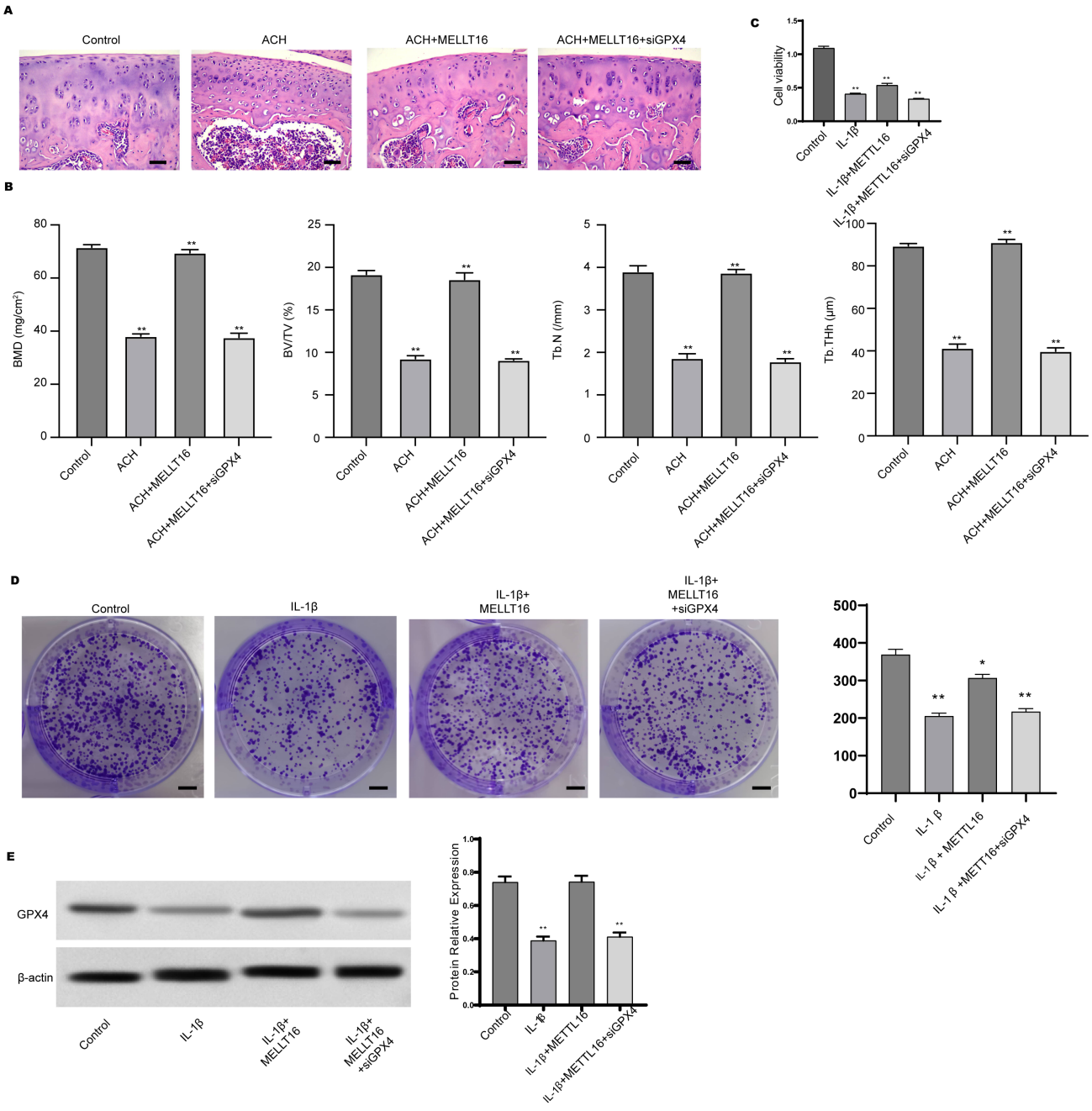

Fig. 6. METTL16 improves chondrogenesis through the regulation of GPX4 expression. (A) H&E staining of proximal tibia tissue. Scale bar = 200 μm. (B) Results for bone mineral density (BMD), bone structure as analyzed by measuring the bone volume to total tissue volume ratio (BV/TV), trabecular number (TbN), and trabecular thickness (TbTh). (C–E) Primary chondrocytes were stimulated with IL-1β and transfected with METTL16 overexpression vectors and siGPX4. (C) Cell viability was measured by the CCK-8 assay. (D) Cell proliferation was detected by colony formation. Scale bar = 200 μm. The GPX4 protein level was detected by Western blotting. (E) GPX4 protein level as assessed by Western blotting. $^{**}p < 0.01$, $^{*}p < 0.05$.

3.6 METTL16 Improves Chondrogenesis by Regulating GPX4 Expression

We further investigated the regulatory role of METTL16/GPX4 in ACH development. The results from H&E staining and bone structure parameters indicated that suppression of GPX4 abolished METTL16-promoted cartilage growth and bone formation (Fig. 6A,B). The results from *in vitro* experiments also revealed that GPX4 knockdown reversed the METTL-16-elevated viability and proliferation of chondrocytes (Fig. 6C,D). The decreased level of GPX4 protein in chondrocytes following siGPX4 transfection was verified by Western blotting (Fig. 6E).

4. Discussion

RNA epigenetic modification has drawn great attention in recent years and has been implicated in multiple biological processes during normal tissue development and disease progression [18,19]. METTL16 is an important m^6A methyltransferase that has been extensively studied in the context of various diseases [20–22]. For example, the level of METTL16 correlates with the progression of glioma [23] and indicates poor prognosis of melanoma [24]. METTL16 was also reported to promote the proliferation of gastric cancer cells via regulation of cyclin D1 expression [25]. Mendel *et al*. [26] reported that METTL16-mediated methylation of structured RNA is essential for the development of mouse embryos. Mechanistic studies have also demonstrated that METTL16 enhances the stability and translational efficiency of PPARγ mRNA by catalyzing its m^6A modification, particularly at the Sequence-1 site. Activated PPARγ induces mitochondrial atrophy and a decrease in membrane potential by reducing the GSH/GSSG ratio and increasing the levels of ROS and MDA, ultimately leading to ferroptosis in BMSCs [27]. The maintenance of cartilage tissue homeostasis relies on the survival, proliferation, and functional activities of chondrocytes, which are the sole cell type in cartilage [28]. Recent studies have demonstrated that ferroptosis, a newly described form of cell death, plays a critical role in cartilage degeneration [29]. However, it is still not known whether METTL16 participates in ACH development. The present work is the first to show that METTL16 improves the ACH syndrome, enhances bone formation, and induces chondrocyte proliferation.

METTL16 was also recently reported to be an important regulator of RNA translation, variable splicing, and stability [18,30]. METTL16 mediates the degradation of MAT2A mRNA, which was disrupted by oxidative stress, which consequently aggravates the apoptosis of nucleus pulposus cells and exacerbates the process of intervertebral disc degeneration [31]. Furthermore, METTL16 mediates the translation of CIDEA in a m^6A-dependent manner and promotes non-alcoholic fatty liver disease [32]. In the current work, we found that METTL16 upregulated the m^6A modification of GPX4 mRNA and suppressed its degradation, thereby increasing the protein level of GPX4. GPX4 is one of the most critical regulators of ferroptosis [33]. As a glutathione peroxidase, GPX4 has been identified to catalyze GSH production and promote ROS clearance [34]. Ferroptosis involves an iron-dependent Fenton reaction that results in the overproduction and buildup of reactive oxygen species (ROS). These ROS can be countered by GPX4, meaning that induction of GPX4 expression is a potential strategy to reduce cell death caused by ferroptosis [35]. Cartilage tissue exists in a hypoxic and avascular microenvironment, with inherently high baseline levels of oxidative stress, making it more prone to rapid accumulation of ROS under pathological conditions [36]. Secondly, chondrocytes have only a weak ability to regulate iron homeostasis. Inflammatory factors can upregulate TfR1, but chondrocytes have only a limited capacity for iron storage and export, resulting in a significantly increased risk of iron overload. Thirdly, the cell membranes of chondrocytes are rich in polyunsaturated fatty acids, providing abundant substrates for lipid peroxidation [37]. Critically, chondrocytes are highly dependent on the GPX4/GSH axis to scavenge lipid peroxides, yet their own capacity for GSH synthesis is limited, rendering this defense system fragile and susceptible to collapse [38]. Consistent with the functions of GPX4 in ferroptosis and cell death, we observed decreased expression of GPX4 in the tibia tissues of ACH transgenic mice. Moreover, we found that suppression of primary chondrocyte ferroptosis by METTL16 was mediated by GPX4. In addition to the GPX4-dependent antioxidant system, ferroptosis can also be regulated through the FSP1–CoQ10 pathway. In the present study, we did not further investigate FSP1 for several reasons. First, accumulating evidence suggests that chondrocytes are highly dependent on the GPX4/GSH axis to counteract lipid peroxidation, whereas FSP1 expression and activity are relatively low or tissue-restricted in cartilage cells. Second, our data showed pronounced alterations in ACSL4, iron metabolism, and GPX4 expression, indicating that lipid remodeling and GPX4 inactivation represent the dominant ferroptotic mechanisms in chondrocytes under inflammatory conditions. Finally, given the limited antioxidant reserve and weak iron-handling capacity of chondrocytes, disruption of the GPX4 pathway is likely sufficient to trigger ferroptosis, making it the primary focus of this study. Nevertheless, future studies exploring potential crosstalk between METTL16 signaling and the FSP1 pathway may further refine our understanding of ferroptosis regulation in cartilage.

5. Conclusion

In summary, our work demonstrated that METTL16 is downregulated during ACH and that overexpression of METTL16 improved bone growth and alleviated the ferroptosis of chondrocytes. Mechanistically, METTL16 increased the m^6A modification of GPX4 mRNA and upregulated its expression in chondrocytes. Our data provided a novel regulatory mechanism for ACH progression.

Availability of Data and Materials

The datasets used or analyzed during the current study are available from the corresponding author on reasonable request.

Author Contributions

LH and XT performed the research and collected experimental data. MY provided technical assistance for experiments, performed the research and sample processing,

and analyzed the data using statistical methods. XMW and XWW analyzed the data using statistical methods. BW designed the study, supervised the research process and provided essential conceptual advice. LH wrote the first draft of the manuscript. All authors contributed to critical revision of the manuscript for important intellectual content. All authors read and approved the final manuscript. All authors have participated sufficiently in the work and agreed to be accountable for all aspects of the work.

Ethics Approval and Consent to Participate

All animal procedures were approved by the Institutional Animal Care and Use Committee (IACUC) of Animal Care and Use Committee of Pediatric Orthopaedic Hospital, Honghui Hospital, Xi'an Jiaotong University (No. KT2023-01-05-01) and conducted in accordance with the relevant guidelines and regulations. This study is reported in accordance with the ARRIVE guidelines (Animal Research: Reporting of In Vivo Experiments). For further details, see: https://arriveguidelines.org.

Acknowledgment

Not applicable.

Funding

This research received no external funding.

Conflict of Interest

The authors declare no conflict of interest.

Supplementary Material

Supplementary material associated with this article can be found, in the online version, at https://doi.org/10.31083/FBL45159.

References

[1] Pauli RM. Achondroplasia: a comprehensive clinical review. Orphanet Journal of Rare Diseases. 2019; 14: 1. https://doi.org/10.1186/s13023-018-0972-6.

[2] Legeai-Mallet L, Savarirayan R. Novel therapeutic approaches for the treatment of achondroplasia. Bone. 2020; 141: 115579. https://doi.org/10.1016/j.bone.2020.115579.

[3] Kumble S, Savarirayan R. Emerging therapies for Achondroplasia: changing the rules of the game. Expert Opinion on Emerging Drugs. 2021; 26: 425–431. https://doi.org/10.1080/14728214.2021.2005577.

[4] Wrobel W, Pach E, Ben-Skowronek I. Advantages and Disadvantages of Different Treatment Methods in Achondroplasia: A Review. International Journal of Molecular Sciences. 2021; 22: 5573. https://doi.org/10.3390/ijms22115573.

[5] Li J, Cao F, Yin HL, Huang ZJ, Lin ZT, Mao N, *et al*. Ferroptosis: past, present and future. Cell Death & Disease. 2020; 11: 88. https://doi.org/10.1038/s41419-020-2298-2.

[6] Pan Q, Luo Y, Xia Q, He K. Ferroptosis and Liver Fibrosis. International Journal of Medical Sciences. 2021; 18: 3361–3366. https://doi.org/10.7150/ijms.62903.

[7] Wu X, Li Y, Zhang S, Zhou X. Ferroptosis as a novel therapeutic target for cardiovascular disease. Theranostics. 2021; 11: 3052–3059. https://doi.org/10.7150/thno.54113.

[8] Hassannia B, Vandenabeele P, Vanden Berghe T. Targeting Ferroptosis to Iron Out Cancer. Cancer Cell. 2019; 35: 830–849. https://doi.org/10.1016/j.ccell.2019.04.002.

[9] Chen X, Kang R, Kroemer G, Tang D. Ferroptosis in infection, inflammation, and immunity. The Journal of Experimental Medicine. 2021; 218: e20210518. https://doi.org/10.1084/jem.20210518.

[10] Liang D, Minikes AM, Jiang X. Ferroptosis at the intersection of lipid metabolism and cellular signaling. Molecular Cell. 2022; 82: 2215–2227. https://doi.org/10.1016/j.molcel.2022.03.022.

[11] Oerum S, Meynier V, Catala M, Tisné C. A comprehensive review of m6A/m6Am RNA methyltransferase structures. Nucleic Acids Research. 2021; 49: 7239–7255. https://doi.org/10.1093/nar/gkab378.

[12] Zhang C, Liu N. N6-methyladenosine (m6A) modification in gynecological malignancies. Journal of Cellular Physiology. 2022; 237: 3465–3479. https://doi.org/10.1002/jcp.30828.

[13] Kumari R, Ranjan P, Suleiman ZG, Goswami SK, Li J, Prasad R, *et al*. mRNA modifications in cardiovascular biology and disease: with a focus on m6A modification. Cardiovascular Research. 2022; 118: 1680–1692. https://doi.org/10.1093/cvr/cvab160.

[14] Wei Y, Li Y, Lu C. Exploring the role of m6A modification in cancer. Proteomics. 2023; 23: e2200208. https://doi.org/10.1002/pmic.202200208.

[15] Shen WB, Ni J, Yao R, Goetzinger KR, Harman C, Reece EA, *et al*. Maternal obesity increases DNA methylation and decreases RNA methylation in the human placenta. Reproductive Toxicology. 2022; 107: 90–96. https://doi.org/10.1016/j.reprotox.2021.12.002.

[16] Su S, Li S, Deng T, Gao M, Yin Y, Wu B, *et al*. Cryo-EM structures of human m^6A writer complexes. Cell Research. 2022; 32: 982–994. https://doi.org/10.1038/s41422-022-00725-8.

[17] Jonquoy A, Mugniery E, Benoist-Lasselin C, Kaci N, Le Corre L, Barbault F, *et al*. A novel tyrosine kinase inhibitor restores chondrocyte differentiation and promotes bone growth in a gain-of-function Fgfr3 mouse model. Human Molecular Genetics. 2012; 21: 841–851. https://doi.org/10.1093/hmg/ddr514.

[18] Pendleton KE, Chen B, Liu K, Hunter OV, Xie Y, Tu BP, *et al*. The U6 snRNA m^6A Methyltransferase METTL16 Regulates SAM Synthetase Intron Retention. Cell. 2017; 169: 824–835.e14. https://doi.org/10.1016/j.cell.2017.05.003.

[19] Ruszkowska A. METTL16, Methyltransferase-Like Protein 16: Current Insights into Structure and Function. International Journal of Molecular Sciences. 2021; 22: 2176. https://doi.org/10.3390/ijms22042176.

[20] Su R, Dong L, Li Y, Gao M, He PC, Liu W, *et al*. METTL16 exerts an m^6A-independent function to facilitate translation and tumorigenesis. Nature Cell Biology. 2022; 24: 205–216. https://doi.org/10.1038/s41556-021-00835-2.

[21] Yoshinaga M, Han K, Morgens DW, Horii T, Kobayashi R, Tsuruyama T, *et al*. The N^6-methyladenosine methyltransferase METTL16 enables erythropoiesis through safeguarding genome integrity. Nature Communications. 2022; 13: 6435. https://doi.org/10.1038/s41467-022-34078-y.

[22] Zhao H, Xu Y, Xie Y, Zhang L, Gao M, Li S, *et al*. m6A Regulators Is Differently Expressed and Correlated With Immune Response of Esophageal Cancer. Frontiers in Cell and Developmental Biology. 2021; 9: 650023. https://doi.org/10.3389/fcell.2021.650023.

[23] Cong P, Wu T, Huang X, Liang H, Gao X, Tian L, *et al*. Identification of the Role and Clinical Prognostic Value of Target Genes of m6A RNA Methylation Regulators in Glioma. Frontiers in Cell and Developmental Biology. 2021; 9: 709022. https://doi.org/10.3389/fcell.2021.709022.

[24] Liu J, Zhou Z, Ma L, Li C, Lin Y, Yu T, *et al*. Effects of RNA methylation N6-methyladenosine regulators on malignant progression and prognosis of melanoma. Cancer Cell International. 2021; 21: 453. https://doi.org/10.1186/s12935-021-02163-9.

[25] Wang XK, Zhang YW, Wang CM, Li B, Zhang TZ, Zhou WJ, *et al*. METTL16 promotes cell proliferation by up-regulating cyclin D1 expression in gastric cancer. Journal of Cellular and Molecular Medicine. 2021; 25: 6602–6617. https://doi.org/10.1111/jcmm.16664.

[26] Mendel M, Chen KM, Homolka D, Gos P, Pandey RR, McCarthy AA, *et al*. Methylation of Structured RNA by the m^6A Writer METTL16 Is Essential for Mouse Embryonic Development. Molecular Cell. 2018; 71: 986–1000.e11. https://doi.org/10.1016/j.molcel.2018.08.004.

[27] Lu L, Wang L, Yang M, Wang H. Role of METTL16 in PPARγ methylation and osteogenic differentiation. Cell Death & Disease. 2025; 16: 271. https://doi.org/10.1038/s41419-025-07527-x.

[28] Li L, Li J, Li JJ, Zhou H, Zhu XW, Zhang PH, *et al*. Chondrocyte autophagy mechanism and therapeutic prospects in osteoarthritis. Frontiers in Cell and Developmental Biology. 2024; 12: 1472613. https://doi.org/10.3389/fcell.2024.1472613.

[29] Zhang Y, Zhang D, Liao X, Xu Q, Bu L, Zheng J, *et al*. Novel insights into the role of ferroptosis in temporomandibular joint osteoarthritis and knee osteoarthritis. International Journal of Medical Sciences. 2025; 22: 2119–2131. https://doi.org/10.7150/ijms.107057.

[30] Doxtader KA, Wang P, Scarborough AM, Seo D, Conrad NK, Nam Y. Structural Basis for Regulation of METTL16, an S-Adenosylmethionine Homeostasis Factor. Molecular Cell. 2018; 71: 1001–1011.e4. https://doi.org/10.1016/j.molcel.2018.07.025.

[31] Chen PB, Shi GX, Liu T, Li B, Jiang SD, Zheng XF, *et al*. Oxidative Stress Aggravates Apoptosis of Nucleus Pulposus Cells through m^6A Modification of MAT2A Pre-mRNA by METTL16. Oxidative Medicine and Cellular Longevity. 2022; 2022: 4036274. https://doi.org/10.1155/2022/4036274.

[32] Tang J, Zhao X, Wei W, Liu W, Fan H, Liu XP, *et al*. METTL16-mediated translation of *CIDEA* promotes non-alcoholic fatty liver disease progression *via* m6A-dependent manner. PeerJ. 2022; 10: e14379. https://doi.org/10.7717/peerj.14379.

[33] Ursini F, Maiorino M. Lipid peroxidation and ferroptosis: The role of GSH and GPx4. Free Radical Biology & Medicine. 2020; 152: 175–185. https://doi.org/10.1016/j.freeradbiomed.2020.02.027.

[34] Forcina GC, Dixon SJ. GPX4 at the Crossroads of Lipid Homeostasis and Ferroptosis. Proteomics. 2019; 19: e1800311. https://doi.org/10.1002/pmic.201800311.

[35] Seibt TM, Proneth B, Conrad M. Role of GPX4 in ferroptosis and its pharmacological implication. Free Radical Biology & Medicine. 2019; 133: 144–152. https://doi.org/10.1016/j.freeradbiomed.2018.09.014.

[36] Hong YH, Park CW, Kim HS, Won KC, Kim YW, Lee CK. Effects of hypoxia/ischemia on catabolic mediators of cartilage in a human chondrocyte, SW1353. Biochemical and Biophysical Research Communications. 2013; 431: 478–483. https://doi.org/10.1016/j.bbrc.2013.01.035.

[37] Wang W, Ma Z, Feng X, Ren J, Sun S, Shao Y, *et al*. TfR1 mediated iron metabolism dysfunction as a potential therapeutic target for osteoarthritis. Arthritis Research & Therapy. 2024; 26: 71. https://doi.org/10.1186/s13075-024-03304-x.

[38] He Q, Lin Y, Chen B, Chen C, Zeng J, Dou X, *et al*. Vitamin K2 ameliorates osteoarthritis by suppressing ferroptosis and extracellular matrix degradation through activation GPX4's dual functions. Biomedicine & Pharmacotherapy. 2024; 175: 116697. https://doi.org/10.1016/j.biopha.2024.116697.